was removed and the crystals were washed with 10 mL of hexane (yield: 0.175 g, 94%). Anal. Calcd for $Mo_2P_2O_4C_{32}H_{58}$: C, 50.53; H, 7.69. Found: C, 51.34; H, 7.66. IR (KBr pellet, cm^{-1}): 2961 (s), 2915 (m), 2863 (m), 1593 (m), 1485 (m), 1449 (w), 1372 (m), 1356 (m), 1321 (m), 1200 (m), 1157 (m), 1119 (s), 994 (s), 955 (s), 830 (m), 793 (w), 745 (m), 762 (m), 635 (s), 577 (m), 531 (w), 448 (w).

Mo_2(O-*i*-Pr)$_4$(dmpe)$_2$. Dmpe (0.104 g, 0.691 mmol) was added to a 20-mL THF solution of $Mo_2(CH_2Ph)_2$(O-*i*-Pr)$_4$ (0.250 g, 0.329 mmol) via syringe. The mixture was stirred at 22 °C under a UV lamp for 2 days. Solvent was removed in vacuo, and hexane was then added to the yellow-brown residue. Cooling to −25 °C yielded two crops of brown microcrystals (yield: 0.200 g, 83%) identified as Mo_2(O-*i*-Pr)$_4$(dmpe)$_2$ by ^1H and ^{31}P NMR spectroscopy.[12]

Crystallographic Studies. General operating procedures and listings of programs have been given previously.[18] A summary of crystal data is given in Table I.

$Mo_2(CH_2Ph)_2$(O-*i*-Pr)$_4$(PMe$_3$) (II). Large well-shaped crystals were present in the submitted sample, and a suitable fragment was cleaved from a representative crystal. After mounting and transferring to the goniostat by using inert atmosphere handling techniques, the crystal was characterized by a reciprocal lattice search technique. A set of diffraction maxima were located which could be indexed as monoclinic, space group $P2_1/c$.

The structure was solved by direct methods (MULTAN78) and Fourier techniques, and refined by full-matrix least squares. All hydrogen atoms were located and refined, although several were poorly behaved. A final difference Fourier was featureless, the largest peak being 0.59 e/Å^3. No absorption correction was performed.

$Mo_2(CH_2Ph)_2$(O-*i*-Pr)$_4$(dmpm) (III). A suitable crystal was selected and transferred to the goniostat using inert atmosphere handling techniques. The crystal was cooled to −168 °C for characterization and data collection.

A systematic search of a limited hemisphere of reciprocal space yielded a set of reflections exhibiting monoclinic symmetry ($2/m$). The systematic extinctions of $0k0$ for $k = 2n + 1$ and of $h0l$ for $h + l = 2n + 1$ uniquely identified the space group as $P2_1/n$. This choice was confirmed by the subsequent solution and refinement of the structure.

The structure was solved by the combination of direct methods (MULTAN) and Fourier techniques. All non-hydrogen atoms were located without difficulty; some of the hydrogen atoms were locatable in a later difference map. All hydrogen atoms were therefore calculated using idealized geometries and a C-H distance at 0.95 Å, they were assigned a fixed B of 1.0 Å^2 plus the isotropic equivalent of the parent atom. The full-matrix least-squares refinement of the structure was completed using anisotropic thermal parameters on all non-hydrogen atoms and fixed hydrogen atoms. Due to the large number of variables (704 total), the refinement was carried out in a cyclical manner. The final R was 0.056; $R_w(F)$ was 0.056.

The asymmetric unit contains two complete molecules, they are labeled A and B, respectively.

The final difference Fourier was essentially featureless, the largest peak was 2 e/Å in the vicinity of C(30)B, indicating a slight disorder in the isopropyl group. No attempts were made at modeling the disorder.

Atomic coordinates for compounds II and III are listed in Tables IV and V, respectively.

Acknowledgment. We thank the National Science Foundation for support.

Supplementary Material Available: Listings of anisotropic thermal parameters and bond distances and angles and VERSORT stereodrawings (12 pages). Ordering information is given on any current masthead page.

OM920242A

(18) Chisholm, M. H.; Folting, K.; Huffman, J. C.; Kirkpatrick, C. C. *Inorg. Chem.* **1984**, *23*, 1021.

Agostic Assistance to Olefin Insertion in Alkylzirconocene Cations: A Molecular Orbital Study by the Extended Hückel Method

Marc-Heinrich Prosenc,† Christoph Janiak,‡ and Hans-Herbert Brintzinger*,†

Fakultät für Chemie, Universität Konstanz, D-7750 Konstanz, Germany, and Kunststofflaboratorium, BASF AG, D-6700 Ludwigshafen, Germany

Received June 9, 1992

Alternative reaction modes for α-olefin insertion in a zirconocene alkyl cation are investigated by the extended Hückel MO method. Agostic interaction of one of the α-H atoms of the migrating alkyl group with the Zr center is found to stabilize the transition state of the preferred reaction mode. Essential contributions to this preference are identified by fragment-MO analysis. Implications of these findings for stereoselective olefin polymerization by chiral *ansa*-metallocene derivatives are discussed.

Introduction

Observations that homogeneous, metallocene-based catalyst systems can induce a stereospecific polymerization of α-olefins[1-3] have opened new possibilities to study the mechanisms of this catalysis, especially the origins of its stereospecificity.[4] Recently, we have reported that olefin insertion into α-deuterated alkyl derivatives of a zirconocene-based polymerization catalyst is influenced in its stereochemistry by kinetic isotope effects.[5] Piers and

* Author to whom correspondence should be addressed.
† Universität Konstanz.
‡ BASF AG. Present address: Institut für Anorganische und Analytische Chemie, Technische Universität Berlin, D-1000 Berlin 12, Germany.

(1) Ewen, J. A. *J. Am. Chem. Soc.* **1984**, *106*, 6355-6364.
(2) Kaminsky, W.; Külper, K.; Brintzinger, H. H.; Wild, F. R. W. P. *Angew. Chem., Int. Ed. Engl.* **1985**, *24*, 507-508.
(3) Reviews: Krentsel, B. A.; Nekhaeva, L. A. *Russ. Chem. Rev.* **1990**, *59*, 1193-1207. Skupinska, J. *Chem. Rev.* **1991**, *91*, 613-648.
(4) Pino, P.; Cioni, P.; Wei, J. *J. Am. Chem. Soc.* **1987**, *109*, 6189-6191.
(5) Krauledat, H.; Brintzinger, H. H. *Angew. Chem., Int. Ed. Engl.* **1990**, *29*, 1412-1413.

0276-7333/92/2311-4036$03.00/0

Bercaw have observed similar isotope effects with scandiocene-based catalysts.[6] These observations imply that these olefin insertions are assisted by an agostic interaction of one of the α-H atoms of the migrating alkyl chain with the metal center, as proposed by Rooney[7] and by Brookhart and Green.[8] To address the question, which Ziegler–Natta catalyst systems are likely to involve such an α-agostic assistance, an understanding of its electronic prerequisites would be desirable.

Olefin insertion in homogeneous catalyst systems[9-16] and α-agostic interaction in electron-deficient metal–alkyl species[17-21] have been subject to MO-theoretical studies in recent years. So far, a clear understanding of the role of agostic interactions in homogeneous Ziegler catalysts has not emerged, however. Recent ab-initio-level studies gave geometries for the lowest-energy transition state which are entirely in accord with an α-agostic interaction between the migrating alkyl group and the metal center.[14-16] One of these studies does indeed ascribe the preference for this transition-state geometry to an α-agostic interaction,[15] but two others see its causes either in steric[14] or in electrostatic[16] interactions.

Molecular orbital studies of the extended Hückel (EHMO) type, while being less precise than ab-initio calculations, differentiate more readily between contributions of different origin, such as specific bonding or repulsive interactions, to overall energy changes. In the following, we utilize this advantage of the extended Hückel method, i.e., the ease with which the influence of individual overlap integrals on MO and total energies can be studied, to delinate the factors which facilitate alternative olefin insertion modes.

Results and Discussion

As in other related studies,[10-16] a cationic zirconocene complex carrying an ethene and a methyl ligand, $[Cp_2Zr(CH_2{=}CH_2)CH_3]^+$, and its transformation to the *n*-propyl complex $[Cp_2ZrCH_2CH_2CH_3]^+$ is considered here as a model for polymer growth by homogeneous Ziegler–Natta catalysts.[22] For this analysis, the geometry of the $(C_5H_5)_2Zr$ fragment is modeled, in a C_{2v}-symmetric conformation, with Zr–C, C–C, and C–H distances of 250, 141, and 100 pm and ring centroid–Zr–centroid and centroid–C–H angles of 130 and 180°, respectively;[23] this geometry (Figure 1) is kept unchanged throughout the following analysis.

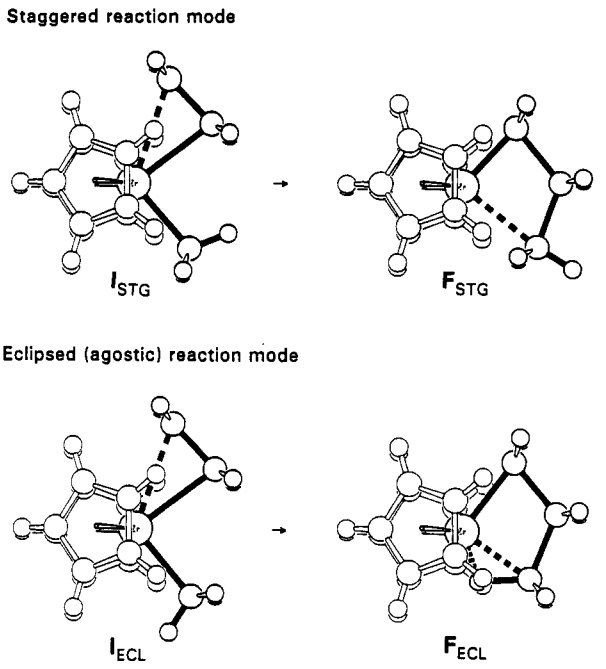

Figure 1. Geometries of initial (I) and final states (F) of olefin insertions by the staggered and the eclipsed reaction modes, as obtained by EHMO energy minimizations (with fixed $(C_5H_5)_2Zr$ fragment geometry).

To study the alternative reaction paths mentioned, two initial-state geometries, I, with overall C_s symmetry have to be considered: a *staggered* geometry, I_{STG}, in which one C–H bond of the CH_3 ligand points between the C–H bonds of the approaching ethene CH_2 group, and an *eclipsed* geometry, I_{ECL}, in which the CH_3 group is rotated by 60° relative to I_{STG} so that two of its C–H bonds are eclipsed with the approaching ethene C–H bonds, while its third C–H bond is in an orientation trans to the ethene ligand, suitable for agostic interaction with the Zr center.

For both of these initial states, the geometries of the methyl and ethene coligands were optimized by an energy-minimum search, using the EHMO procedure[24] described in the Computational Appendix. For this optimization procedure, all three C ligand atoms were kept in the metallocene midplane, i.e. in the plane bisecting the centroid–Zr–centroid angle.

While the geometries and energies computed in this manner should not be viewed as accurate in a quantitative sense, the following qualitative observations pertain to the alternative initial-state species I_{STG} and I_{ECL} (Figure 1, left).

(1) The two conformers differ little in their total energies, I_{ECL} being lower than I_{STG} by ca. 10 kJ/mol. (2) Both

(6) Piers, W. E.; Bercaw, J. E. *J. Am. Chem. Soc.* **1990**, *112*, 9406–9407.
(7) Laverty, D. T.; Rooney, J. J. *J. Chem. Soc., Faraday Trans.* **1983**, *79*, 869–878.
(8) Brookhart, M.; Green, M. L. H. *J. Organomet. Chem.* **1983**, *250*, 395–408. Brookhart, M.; Green, M. L. H.; Wong, L. *Prog. Inorg. Chem.* **1988**, *36*, 1–124.
(9) Armstrong, D. R.; Perkins, P. G.; Steward, J. J. P. *J. Chem. Soc., Dalton Trans.* **1972**, 1972–1980.
(10) Lauher, J. W.; Hoffmann, R. *J. Am. Chem. Soc.* **1976**, *98*, 1729 1742. Thorn, D. L.; Hoffmann, R. *J. Am. Chem. Soc.* **1978**, *100*, 2079–2090.
(11) Novaro, O.; Blaisten-Barojas, E.; Clementi, E.; Giunchi, G.; Ruiz-Vizcaya, M. E. *J. Chem. Phys.* **1978**, *68*, 2337–2351.
(12) Fujimoto, H.; Yamasaki, T.; Mizutani, H.; Koga, N. *J. Am. Chem.* **1985**, *107*, 6157–6161.
(13) Shiga, A.; Kawamura, H.; Ebara, T.; Sasaki, T.; Kikuzono, Y. *J. Organomet. Chem.* **1989**, *366*, 95–104.
(14) Jolly, C. A.; Marynick, D. S. *J. Am. Chem. Soc.* **1989**, *111*, 7968–7974.
(15) Kawamura-Kuribayashi, H.; Koga, N.; Morokuma, K. *J. Am. Chem. Soc.* **1992**, *114*, 2359–2366. Koga, N.; Morokuma, K. *Chem. Rev.* **1991**, *91*, 823–842.
(16) Castonguay, L. A.; Rappé, A. K. *J. Am. Chem. Soc.* **1992**, *114*, 5832–5842.
(17) Obara, S.; Koga, N.; Morokuma, K. *J. Organomet. Chem.* **1984**, *270*, C33–C36. Koga, N.; Obara, S.; Morokuma, K. *J. Am. Chem. Soc.* **1984**, *106*, 4625–4626.
(18) Eisenstein, O.; Jean, Y. *J. Am. Chem. Soc.* **1985**, *107*, 1177–1186.
(19) Calhorda, M. J.; Simoes, J. A. M. *Organometallics* **1987**, *6*, 1188–1190.
(20) Tatsumi, K.; Nakamura, A. *J. Am. Chem. Soc.* **1987**, *109*, 3195–3206; *Organometallics* **1987**, *6*, 427–428. Mashima, K.; Nakamura, A. *J. Organomet. Chem.* **1992**, *428*, 49–58.
(21) Shiga, A.; Kojima, J.; Saski, T.; Kikuzono, Y. *J. Organomet. Chem.* **1988**, *345*, 275–285.
(22) Zirconocene cations in homogeneous Ziegler catalysis: Jordan, R. F. *Adv. Organomet. Chem.* **1991**, *32*, 325–387 and references quoted there.
(23) Structural data of $(C_5H_5)_2Zr$ derivatives: Orpen, A. G.; Brammer, L.; Allen, F. H.; Kennard, O.; Watson, D. G.; Taylor, R. *J. Chem. Soc., Dalton Trans.* **1989**, S1–S83 and references quoted there.
(24) (a) Hoffmann, R. *J. Chem. Phys.* **1963**, *39*, 1397–1412. Hoffmann, R.; Lipscomb, W. N. *Ibid.* **1962**, *36*, 2179–2189; **1962**, *37*, 2872–2883. (b) Howell, J.; Rossi, A.; Wallace, D.; Haraki, K.; Hoffmann, R. Forticon8. Quantum Chemical Program Exchange, Indiana University, Bloomington, IN 47405.

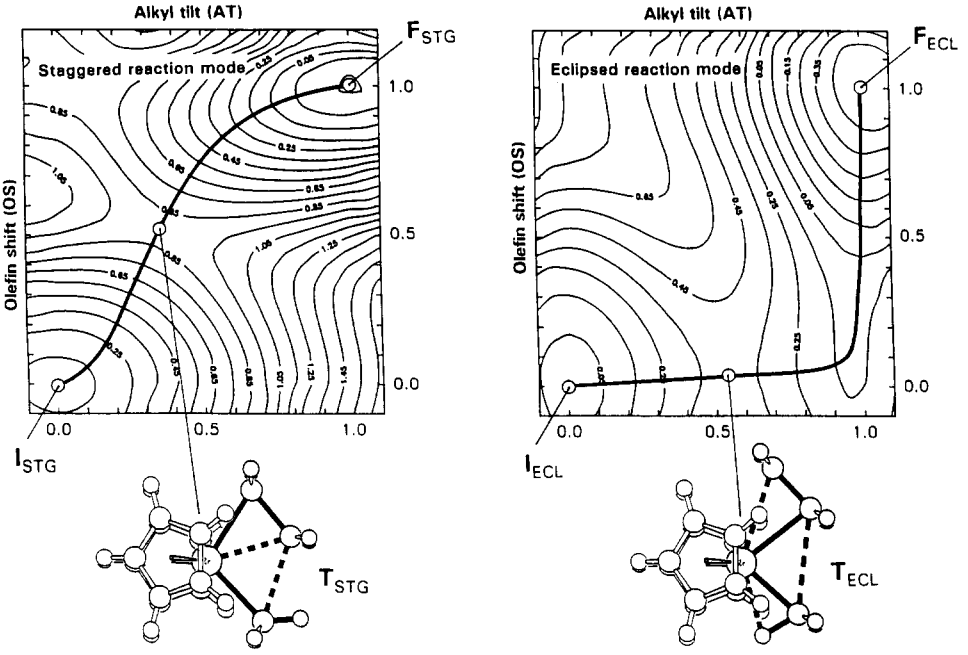

Figure 2. Energy surfaces with respect to alkyl tilt and olefin shift reaction coordinates, insertion reaction paths, and transition-state geometries for the staggered and the eclipsed reaction modes.

species contain an unsymmetrically bound ethene ligand: The centrally located CH_2 terminus is found 256 pm from the Zr atom; its charge is practically nil. The lateral terminus, on the other hand, is located 286 pm from the Zr atom and carries a positive charge of 0.17 units.[25] (3) For both geometries, the local C_3 axis of the CH_3 group coincides with the Zr–C bond axis. A prevalence of repulsive interactions between the Zr atom and the H(α) atoms of I_{STG} and I_{ECL} is indicated by the observation that the total energies of these species are decreased if the Zr–H(α) overlap is set to zero.

The geometries of the two "final" states F_{STG} and F_{ECL} are derived from those of I_{STG} and I_{ECL}, respectively, by bringing the central olefin terminus and the CH_3 group into bonding contact, while the ethene and the methyl C atoms in the midplane of the complex are kept so as to maintain an overall C_s symmetry.[27] The geometries thus obtained for F_{STG} and F_{ECL} by an EHMO energy minimization (Figure 1, right) are remarkable again in several respects: (1) The alternative final-state conformers F_{STG} and F_{ECL} differ substantially in their total energies: The eclipsed conformer F_{ECL} yields an energy lower by ca. 35 kJ/mol than the staggered conformer F_{STG}. (2) For F_{ECL}, the midplane H atom at the γ-CH_3 end of the newly formed *n*-propyl chain is found only 196 pm from the Zr atom; this indicates that an agostic interaction of a γ-C–H bond with the Zr center contributes to the extra stability of this species. Accordingly, the total energy of species F_{ECL} rises dramatically (by ca. 95 kJ/mol) if the Zr–H(γ) overlap is set to zero. (3) In the staggered product species F_{STG}, two H atoms of the γ-CH_3 group are located 252 pm from the Zr center. These Zr–H interactions can hardly be bonding, however, since the energy of F_{STG} *falls* by ca. 2.5 kJ/mol if the Zr–H(γ) overlap integrals are set to zero. A fragment MO analysis (to be discussed below) shows that the γ-CH_3 group is bound to the Zr center by transfer of electron density from the C(β)–C(γ) σ bond into Zr orbitals of symmetry a′.

The increased weight of agostic interactions for the final states F_{ECL} and F_{STG} as compared to their predecessors I_{ECL} and I_{STG} is undoubtedly connected with their increased electron deficiency: while $[Cp_2Zr(CH_2{=}CH_2)\text{-}CH_3]^+$ has the 16-electron configuration typical for many Cp_2ZrX_2 derivatives, a final species $[Cp_2ZrCH_2CH_2CH_3]^+$ would have an unprecedented 14-electron configuration and must thus be critically dependent on some agostic stabilization. Such an agostic stabilization is provided, more efficiently than by the Zr←H(α) interactions discussed above, by the γ-CH bonds present in this final species.[19] Both empty metal orbitals of this species are of a′ symmetry and are located in the midplane of the molecule.[10] Any γ-agostic stabilization must thus be much greater for conformer F_{ECL}, since its γ-CH bond approaches the Zr atom in this electron-deficient midplane. In F_{STG} on the other hand, the two γ-C–H bonds approaching the Zr center above and below the molecular midplane will suffer repulsion by occupied MOs of symmetry a″, which are mainly of cyclopentadienyl π-character.

To obtain further insights with regard to the reaction paths leading from I_{STG} to F_{STG} and from I_{ECL} to F_{ECL}, we have constructed a highly simplified, two-dimensional energy surface by aggregating the geometry changes as-

(25) Similarly unsymmetric coordination of ethene to $(C_5H_5)_2ZrCH_3^+$ and $Cl_2ZrCH_3^+$ fragments, with a more positive charge on the lateral than on the central ethene terminus, has also been observed in ab-initio studies.[14-16] During the insertion/migration reaction about 0.5 charge units are transferred from the CH_3 ligand to the lateral CH_2 terminus, which thus becomes distinctly anionic, while the central CH_2 terminus remains practically without charge. In this regard, the olefin insertion studied here deviates from β-H transfer in related metallocene complexes, where a partial positive charge has been found to arise at the (central) β-CH_2 terminus.[26]

(26) Doherty, N. M.; Bercaw, J. E. *J. Am. Chem. Soc.* **1985**, *107*, 2670–2682.

(27) Not considered here are possible distortions of these product structures (and the corresponding transition-state species) from C_s symmetry. While titanacyclobutane derivatives, which are formally related to these species by loss of a proton, show very little deviation from coplanarity of the four-membered metallacycle,[28-30] a preference for non-coplanar transition-state geometries has been reported in ref 15.

(28) Lee, J. B.; Gajda, G. J.; Schaefer, W. P.; Howard, T. T.; Ikariya, T.; Straus, D. A.; Grubbs, R. H. *J. Am. Chem. Soc.* **1981**, *103*, 7358–7361. Grubbs, R. H.; Tumas, W. *Science* **1989**, *243*, 907–915.

(29) Eisenstein, O.; Hoffmann, R.; Rossi, A. *J. Am. Chem. Soc.* **1981**, *103*, 5582–5584.

(30) Rappé, A. K.; Goddard, W. A., III. *J. Am. Chem. Soc.* **1982**, *104*, 297–299. Upton, T. J.; Rappé, A. K. *Ibid.* **1985**, *107*, 1206–1218.

sociated with these transformations into two reaction coordinates, one involving all geometry changes at the CH_3 group and the other one all those at the olefin ligand (cf. Figure 1). In each case the CH_3 group has to tilt away from the Zr–C bond axis and to shift slightly toward the inner ethene terminus. The ethene moiety has to shift toward the methyl group while undergoing a lengthening of its C=C bond and a rehybridization at both CH_2 termini. Each of these two aggregated reaction coordinates, to be called for short "alkyl tilt" (AT) and "olefin shift" (OS), were scaled to range from 0 to 1. The geometries of I_{STG} and I_{ECL} are thus defined as AT(0.0)/OS(0.0), and those of F_{STG} and F_{ECL}, as AT(1.0)/OS(1.0). All angular and bond length changes associated with a given reaction coordinate were divided into 20 equal steps. Two-dimensional energy surfaces ranging from AT(−0.25)/OS(−0.25) to AT(1.25)/OS(1.25) were determined by calculating total energies for each of the 31·31 intermediate geometries by standard EHMO methods. While this analysis is certainly reliable only in a qualitative sense, it provides, again, a clear distinction between the two reaction modes.

The energy surface thus obtained for the staggered reaction mode yields a reaction path in which alkyl tilt and olefin shift proceed in a concerted manner. It leads to a transition state T_{STG} with a geometry close to AT(0.4)/OS(0.5) and a calculated activation energy of 85 kJ/mol (Figure 2, left). The energy surface for the eclipsed reaction mode, on the other hand, is quite unsymmetrical: The first phase of the reaction path involves almost exclusively a tilting of the methyl group; it leads through a transition state T_{ECL} with a geometry close to AT(0.5)/OS(0.0).[31] In the second phase of this reaction path, the olefin shifts into its final position with hardly any further motion of the methyl group (Figure 2, right).

This biphasic reaction path thus involves a transition state which contains the CH_3 group in an agostically distorted geometry similar to that observed in the final product. Electron deficiency at the metal center, which must rise along the reaction path, appears to reach a substantial measure already at the transition state. As the stabilization of such a species by agostic coordination of a C–H bond requires that the latter is located in the midplane of the reaction complex, a smaller activation energy is to be expected for T_{ECL} than for T_{STG}. The activation energy of ca. 37 kJ/mol calculated for T_{ECL} is indeed lower by ca. 50 kJ/mol than that obtained for T_{STG}.

The same conclusion is reached if one considers the changes induced by deletion of Zr–H(α) overlaps in the energy profiles of both reaction paths. Relative energies, calculated with normal and with deleted Zr–H overlap, show that Zr–H interactions are destabilizing in both initial states, due to a preponderantly antibonding overlap between H and Zr orbitals in the MOs associated with the Zr–CH_3 bond. This destabilization is diminished as the reaction proceeds along either reaction path. It never quite vanishes, however, for the staggered reaction mode (Figure 3, top). For the eclipsed reaction mode, on the other hand, destabilization by the Zr–H interaction vanishes more rapidly along the reaction path and is transformed into a strong stabilization in its later part. A net stabilization of the reaction complex arises just close to the transition

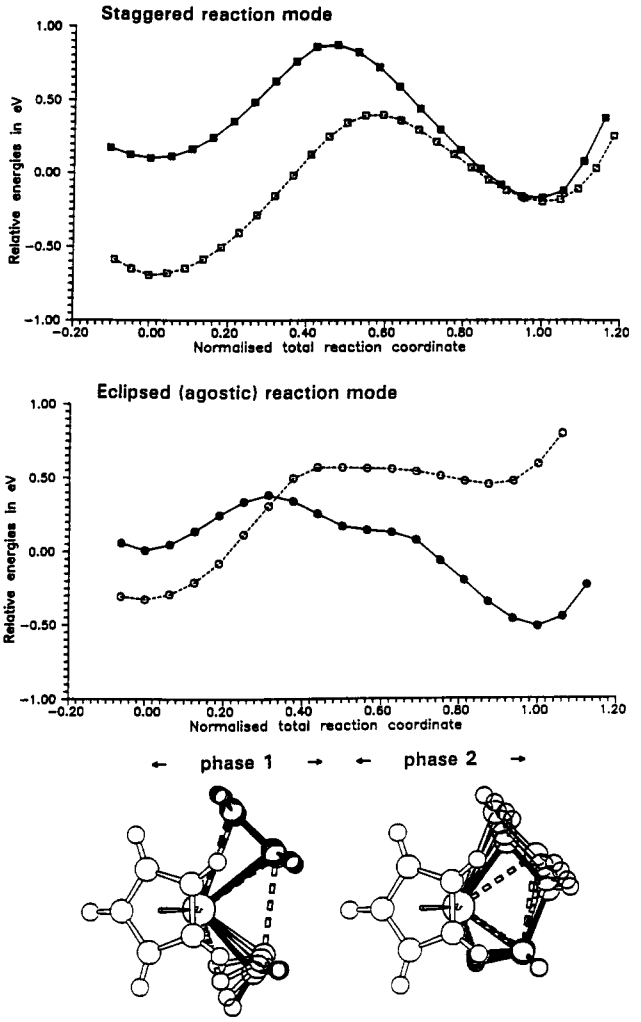

Figure 3. Energy changes (relative to I_{ECL}) along the reaction path for the staggered and the eclipsed reaction modes, calculated with normal (■) and with deleted (□) Zr–H(α) overlap integrals, and motions of the CH_3 and C_2H_4 units during phases 1 and 2 of the agostic reaction mode.

state (Figure 3, bottom). Obviously, transition state T_{ECL} is favored over T_{STG} by the same type of Zr–H interactions which favor the final insertion product F_{ECL} over F_{STG}.

The preceding analysis does not depend in a critical manner on the choice of parameters: Qualitatively similar reaction paths with differently positioned transition states are obtained if different parameters are employed, e.g. for the Zr 4d orbital energies.[31]

Contributions of crucial MOs to the overall energy change along the biphasic, agostic insertion path can be followed in more detail by Walsh diagrams associated with the alkyl tilt and olefin shift coordinates in an even more simplified model complex $[H_2Zr(C_2H_4)CH_3]^+$ (Figure 4):[32] The HOMO represents the initial Zr—CH_3 bond; it rises in energy when the CH_3 group is tilted. This energy rise stems in part from a loss of Zr–C overlap and in part from an increasingly antibonding Zr–H contribution to this MO (documented by a decrease in energy upon deletion of the Zr–H overlap). Similar observations on Cl_3TiCH_3 are reported in ref 18. This unfavorable effect of an alkyl tilt on the HOMO is partly compensated, however, by an energy gain of MOs 1a′ and 2a′, which is caused by in-

(31) As this alkyl tilt is quite exergonic in the region 0.5 < AT < 1.0, an α-agostically distorted species might even be an intermediate in the olefin insertion reaction sequence. With a Zr 4d orbital energy of −11.6 eV (standard EHMO procedure for geometry optimization and energy surface computation), two transition states at AT(∼0.5)/OS(∼0.0) and AT(∼0.9)/OS(∼0.4) and a shallow energy minimum at AT(∼0.9)/OS(∼0.0) are indeed found along the agostic reaction path described in Figure 4.

(32) We have chosen this highly simplified model for the FMO analysis to concentrate the essential MOs in a limited number of fragment orbitals. We find that the MO level ordering for a $(C_5H_5)_2Zr$ fragment is reproduced better by a H_2Zr than by a Cl_2Zr fragment.

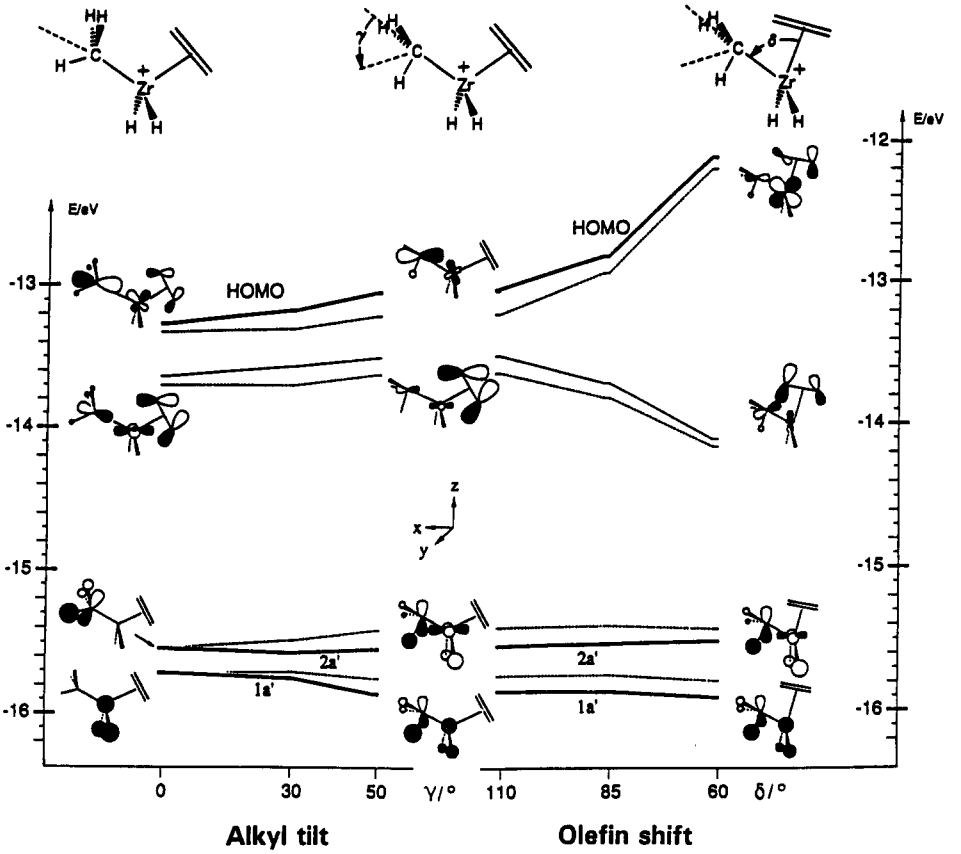

Figure 4. Walsh diagrams for essential MOs of a $H_2Zr(C_2H_4)CH_3^+$ model species for variations of the alkyl tilt angle γ and of the olefin shift angle δ. Solid lines represent results obtained with normal overlap integrals and dotted lines those obtained with deleted Zr–H overlap integrals.

creasing agostic interactions of the α-C–H bond with the Zr 5s and $4d_{x^2-y^2}$ orbitals.

In the second insertion phase, the HOMO represents the incipient σ-bond between the lateral olefin terminus and the Zr center, the next highest MO being the newly formed C–C σ-bond. Part of the electron density of this new C–C bond is retained in a d_{z^2}-type orbital of the Zr atom, in accord with the notion that the metal center is highly electron deficient at this stage of the reaction path. Throughout phase 2, the reaction complex maintains the agostic stabilization, gained in phase 1 by the interaction of one of the C–H bonds of the terminal CH_3 group with a a′-symmetric 5s and $4d_{x^2-y^2}$ orbitals of the Zr atom.

While the preceding analysis can be assumed to give an appropriate picture of the way in which agostic interactions facilitate the insertion of olefins into cationic alkylzirconocene species, a caveat appears necessary: Whenever the electron deficiency of the reaction complex is relieved by some external ligand species, the agostic reaction mode would undoubtedly lose most of its advantage.

Conditions of this kind are e.g. coordination of a second olefin ligand to the Zr center before or during the insertion step[33] or maintenance of residual bonding to the counteranion even in the insertion transition state.[34-36] While difficult to reconcile with existing geometrical constraints, especially in sterically crowded metallocenes,[37] stabilization

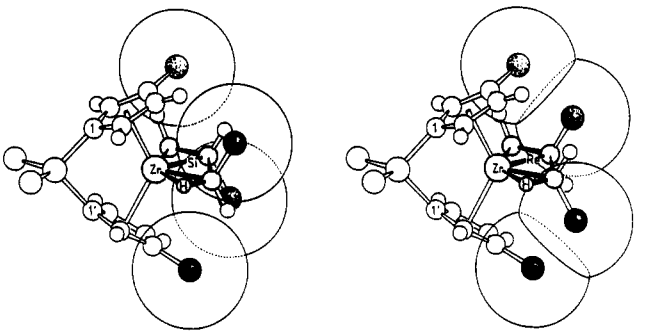

Figure 5. Alternative transition states for the insertion of propene in a chiral *ansa*-metallocene alkyl cation. Methyl groups are represented by spherical van der Waals outlines with R = 1.9 Å.

of the otherwise electron-deficient transition state by an external ligand (instead of an internal Zr←H interaction) cannot be excluded a priori in all cases. Whether α-agostic assistance is at work in a particular catalyst system will thus have to be decided experimentally, e.g. by kinetic isotope effects exerted by an α-CHD group on the insertion stereochemistry.[38]

(33) Ystenes, M. *J. Catal.* **1991**, *129*, 383–401 and references quoted there.
(34) Hlatky, G. G.; Turner, H. W.; Eckman, R. R. *J. Am. Chem. Soc.* **1989**, *111*, 2728–2729.
(35) Yang, X.; Stern, C. L.; Marks, T. J. *J. Am. Chem. Soc.* **1991**, *113*, 3623–3625.
(36) Eisch, J. J. *Makromol. Chem.*, in press, and references quoted there.
(37) Hortmann, K.; Brintzinger, H. H. *New J. Chem.* **1992**, *16*, 51–55.
(38) Preliminary studies, by means of the ICONC version of the EHMO procedure, developed by Calzaferri to include core–core-repulsion terms,[39] on changes in the Morse potentials of α-C–H bonds along the agostic reaction coordinate, indicate that the stretching force constant of the Zr-bound C–H bond is reduced to ca. 75% of its initial value in the transition state T_{ECL}. A ratio of $k_H/k_D \approx 1.25$ is thus expected for Zr←H–C relative to Zr←D–C stabilized transition states in reasonable agreement with experimentally observed values.[5,6]
(39) Calzaferri, G.; Forss, L.; Kamber, I. *J. Phys. Chem.* **1989**, *93*, 5366–5371.

Table I. Extended Hückel Parameters

atom	orbital	orbital exponents	H_{ii}	ref
Zr	5s	1.817	−9.87	43
	5p	1.776	−6.76	
	4d	3.835 (0.6211)[a]	−11.18	
		1.505 (0.5796)[a]		
C	2s	1.625	−21.40	24
	2p	1.625	−11.40	
H	1s	1.300	−13.60	24

[a] Coefficients used in the double-ζ expansion of the d orbitals.

If supported by further evidence, the picture of the olefin insertion step presented above would greatly simplify our understanding of stereoselectivity in olefin polymerization catalysis: Of the two conceivable conformers of the Zr–CH_2 unit, with either one of the two α-H atoms agostically bound to the Zr center, one appears to be entirely compatible with the steric requirements of the substituted ligand framework of a typical chiral *ansa*-metallocene catalyst (Figure 5, left). A Zr←H–C interaction involving the "wrong" α-H atom, on the other hand, would lead to prohibitive repulsive contacts between the disubstituted β-C atom of the polymer chain and the β-substituent of the ligand framework (Figure 5, right). This geometry thus appears inaccessible for steric reasons. Since the substituted olefin terminus approaches the α-CH_2 group of the polymer in an eclipsed mode, the formation of the new C–C bond must, furthermore, be strictly contingent on a trans disposition of the two alkyl substituents which flank the incipient C···C bond. The increased rigidity conferred on the insertion transition state by the Zr←H–C interaction thus provides a reasonable explanation for the high degrees of stereoselectivity generally associated with these olefin polymerization catalysts.

The preferred transition-state geometry for stereoregular α-olefin insertions, as derived from the agostic reaction mode described above, is remarkably similar to that obtained by Corradini and co-workers from an analysis of van der Waals repulsion terms alone.[40] This supports our notion that the agostic reaction mode does indeed fulfill steric as well as electronic requirements for typical chiral *ansa*-metallocenes with one unsubstituted β-position at each ring. For catalytic systems involving sterically more strongly encumbered metallocenes, such as permethylzirconocene derivatives, we would anticipate that α-agostic assistance can no longer operate for steric reasons and that alternative transition states take over.

A related question concerns the reaction mode(s) by which the generally small but temperature-sensitive fraction of stereoerrors arises in these homogeneous catalyst systems. An α-agostic transition state involving incorrect enantiofacial orientation of the inserting olefin appears highly unlikely for the reasons discussed above. The possibility that structurally more flexible (albeit energetically less favorable) nonagostic transition states are responsible for the occurrence of these stereoerrors thus warrants further examination. Electronic effects on the stereoselectivity of zirconocene-catalyzed propene polymerizations, which are in accord with this view, have recently ben published by Collins and co-workers.[41]

Acknowledgment. We thank Kai Hortmann and Peter Burger, University of Konstanz, for help with early stages of this work. Financial support by the VW Foundation, Fonds der Chemie, and funds of the University of Konstanz, as well as a donation by the Freunde der TU Berlin, are gratefully acknowledged. C.J. thanks BASF AG, Ludwigshafen, Germany, Division ZKP, for the award of a postdoctoral fellowship and for support of this work.

Computational Appendix

Energy surface and Walsh diagram calculations were done with the standard extended Hückel method,[24] using the H_{ii} values given in Table I, weighted H_{ij} values,[42] and a value of 1.75 for the Hückel constant. While the geometry of the $(C_5H_5)_2Zr$ fragment was kept unchanged at the parameters specified above, all bond distances and angles involving the CH_3 and C_2H_4 ligands were varied to find the minimal-energy geometries for the initial and final species; for these geometry optimizations, Calzaferri's version of the EHMO procedure[39] was employed.

OM920331N

(40) Corradini, P.; Guerra, G.; Vacatello, M.; Villani, V. *Gazz. Chim. Ital.* **1988**, *118*, 173–177. Corradini, P.; Guerra, G. *Prog. Polym. Sci.* **1991**, *16*, 239–257. Corradini, P. *Makromol. Chem.*, in press, and references quoted there.

(41) Lee, I. M.; Gauthier, W. J.; Ball, J. M.; Iyengar, B.; Collins, S. *Organometallics* **1992**, *11*, 2115–2122.

(42) Ammeter, J. H.; Bürgi, H. B.; Thibeault, J. C.; Hoffmann, R. *J. Am. Chem. Soc.* **1978**, *100*, 3686–3692.

(43) Tatsumi, K.; Nakamura, A.; Hofmann, P.; Stauffert, P.; Hoffmann, R. *J. Am. Chem. Soc.* **1985**, *107*, 4440–4451.